Tuning the Electrochemical and Photophysical Properties of Osmium Complexes for Application in Photoredox Catalysis

Samantha L. Goldschmid[a]
Eva Bednářová[a, #]
Logan R. Beck[a, #]
Katherine Xie[a]
Nicholas E. S. Tay[a]
Benjamin D. Ravetz[a]
Jun Li[b]
Candice L. Joe[b]
Tomislav Rovis*[, a]

[a] Department of Chemistry, Columbia University, New York, New York 10027, United States

[b] Chemical Process Development, Bristol Myers Squibb, New Brunswick, New Jersey 08903, United States

[#] These authors contributed equally.

tr2504@columbia.edu

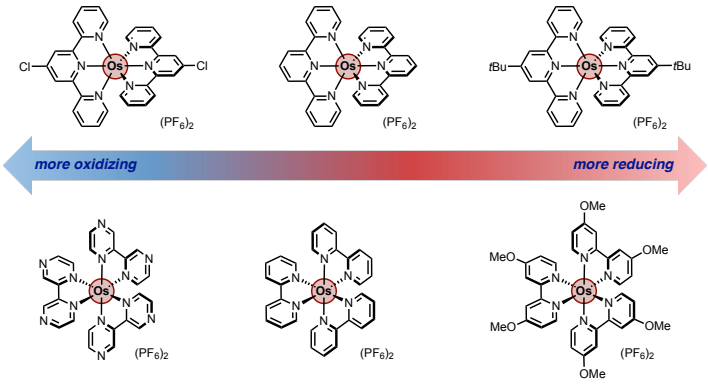

Received:
Accepted:
Published online:
DOI:

Abstract Photocatalysis driven by visible and ultraviolet irradiation is a fundamental tool for synthetic chemists. Recently, expansion of this tool to near-infrared (NIR) light has gained in popularity. Herein, we report the detailed photophysical characterization of a library of Os^{II} polypyridyl photosensitizers that absorb NIR irradiation. By tuning ligand scaffold and electron density, we access a range of synthetically useful excited state energies and redox potentials.

Key words photoredox catalysis, near-infrared, ligand design

1 Introduction

1.1 Scope

Photoredox catalysis has emerged as an important tool for synthetic, medicinal, process, and materials chemists alike. [1] Most state-of-the-art photoredox catalysts today are metal complexes or organic dyes which absorb high energy visible light to generate an excited state capable of acting as a potent single-electron donor, acceptor, or triplet sensitizer.[2] Recently, our group and others have explored a different modality of photoredox catalysis: one which utilizes lower energy near-infrared (NIR) light to generate these reactive excited states.[3,4,5]

NIR photoredox catalysis is a complementary method to traditional photoredox catalysis in that it offers access to products which may be inaccessible with high energy visible-light photoredox catalysis. Substrates with extended pi-systems or photolabile functionalities may competitively absorb the incident light, which could lead to photocatalyzed substrate decomposition. Additionally, the depth to which NIR light can penetrate various barriers such as biological tissue is greater, allowing for catalysis *in vivo*.[5] Finally, photoredox catalysis is generally energetically inefficient, due to the thermal relaxation *via* intersystem crossing that the excited singlet must undergo in order to reach the catalytically active triplet state. However, due to strong spin-orbit coupling, osmium-based photocatalysts undergo spin-forbidden excitation to directly reach the triplet state upon irradiation with NIR light. Due to the relatively low extinction coefficient of this transition relative to that of the ground state to singlet transition, the incident NIR light can penetrate further into the reaction flask, allowing for photoredox catalysis in batch at mole-scale.[4] Thus, osmium-complex-catalyzed NIR photoredox catalysis offers energetically efficient catalysis which may be compatible with photo-labile functionalities and could be used in applications on scale and in biological systems.

Polypyridyl complexes of osmium were first synthesized and characterized in the 1940's and 50's,[6] and have since been studied in various applications including dye-sensitized solar cells,[7] as biological probes,[8] and binuclear complexes.[9] Previously, our group developed several osmium-based photocatalysts and demonstrated their competency at carrying out various transformations with NIR irradiation.[4] As the ability of these chromophores to achieve reactivity previously only accomplished with near-UV or visible light has now been established, our next goal is to develop a library of catalysts with a wide range of electrochemical properties in order to facilitate the adoption of NIR photoredox catalysis to a broader scope of reactions. Additionally, by identifying the ways in which the electronic structure of the ligands in our library affects the electrochemical and photophysical properties of these complexes, we hope that this manuscript may be used as a guide for future ligand design.

1.2 Measuring Ground-State Redox Potentials

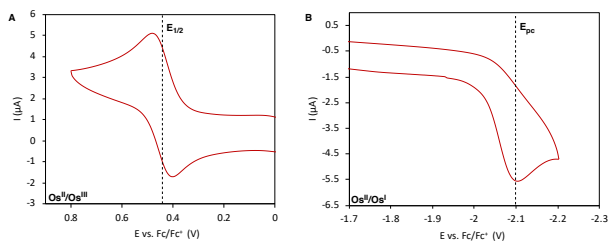

Figure 1 A) Reversible $Os^{II/III}$ oxidation wave B) Irreversible $Os^{II/I}$ reduction wave.

Ground-state redox potentials are measured using cyclic voltammetry (CV). For a reversible redox event, an anodic and cathodic wave are observed, where the standard potential of the reaction is reported as $E_{1/2}$, or halfway between the anodic and cathodic peak currents. At $E_{1/2}$, [ox] = [red] at the electrode surface (Figure 1A).[11] For an irreversible redox event, no return wave is observed. Thus, an $E_{1/2}$ value cannot be calculated. In these cases, we take E_{pc} as the value for the formal potential (Figure 1B).

Redox potentials measured in CV must be reported relative to a known reference. While many common aqueous reference electrodes are frequently used to characterize photocatalysts, these are not ideal for measuring accurate redox potentials in organic solvents.[13] This is due to the junction potential which may arise when the aqueous electrolyte diffuses into the organic solution and *vice versa*.[12] The electrochemical data for these experiments were collected in acetonitrile with tetrabutylammonium hexafluorophosphate ($TBAPF_6$) as supporting electrolyte. Thus, all redox potentials were referenced to the ferrocene/ferrocenium (Fc/Fc^+) couple using a pseudo reference electrode and ferrocene as an internal standard.

1.3 Measuring Photophysical Properties

Once the ground state redox potentials are determined, the photophysical properties of the chromophore must be measured. The energy of the transitions from the ground state (S_0) to first excited singlet (S_1) and ground state to first excited triplet (T_1) determines the wavelengths of incident light which can be used to excite an electron to these states. Additionally, in order to effectively absorb the incident light and be appreciably promoted to its excited state, the chromophore must have a sufficiently high extinction coefficient at the wavelength of irradiation. In order to probe these properties, UV-visible spectroscopy is employed. As described by the Beer-Lambert Law, the absorbance (A) of a given solution is directly dependent upon the path-length (ℓ), the extinction coefficient (ε), and the concentration (c) of the analyte (Equation 1).

$$A = \varepsilon c \ell$$

Equation 1 The Beer-Lambert Law

Thus, by measuring the UV-visible spectrum of each chromophore and using the Beer-Lambert Law to determine their extinction coefficients at various wavelengths, we can determine which wavelengths of light can be used to excite each chromophore and how effectively each chromophore will absorb that light (Figure 2).

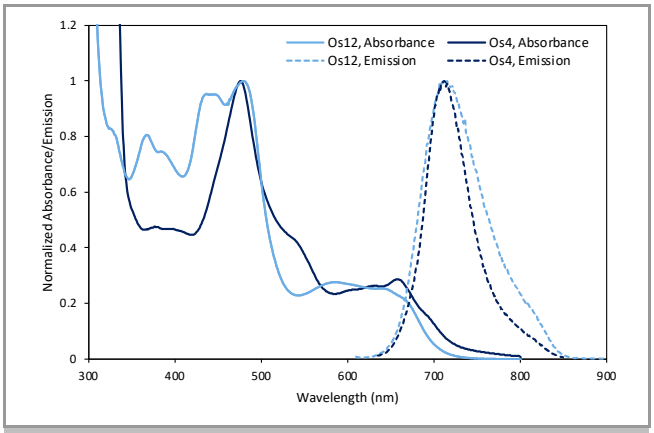

Figure 2 Comparison of normalized absorption and emission spectra for complex **Os12** ($[Os^{II}(bpy)_3](PF_6)_2$) and complex **Os4** ($[Os^{II}(tpy)_2](PF_6)_2$).

The photophysical properties are also vital for determining the excited-state redox potentials of a photocatalyst. Excited-state redox potentials ($E^*_{1/2}$) are commonly estimated using the Rehm-Weller equation, in which the ground state redox potentials ($E_{1/2}$) are adjusted using the vibrational zero-point energy ($E_{0,0}$) (Equations 2 and 3).[14]

$$(2)\ E^{*\,red}_{1/2} = E^{red}_{1/2} + E_{0,0} + \omega_r$$

$$(3)\ E^{*\,ox}_{1/2} = E^{ox}_{1/2} - E_{0,0} + \omega_r$$

Equations 2 and 3 The Rehm-Weller Equation for estimating excited-state reduction (2) and oxidation (3) potentials.

The electrostatic work term (ω_r) describes charge separation within the electron-transfer complex and is considered negligible.[15] Determining an accurate value for $E_{0,0}$ is key in estimating these excited-state potentials. Ideally, $E_{0,0}$ can be determined empirically by measuring the emission spectrum at 77 K.[16] If access to this type of instrumentation is not possible, $E_{0,0}$ is commonly approximated. Many methods to estimate $E_{0,0}$ have been previously reported, including using A) the wavelength of the emission maximum,[17] B) the intersection of the normalized absorption and emission spectra,[18] C) the x-intercept at 10% of the maximum height on the blue-shifted side of the emission spectrum,[19] and D) the x-intercept of the tangent line drawn at the inflection point of the blue-shifted side of the emission spectrum[20] (Figure 3). We compared these estimation methods with reported 77K $E_{0,0}$ values of known osmium complexes in the literature. Based on this analysis, we have decided to take the lambda max of emission as the best estimate of $E_{0,0}$ for OsL_3-type complexes, while the tangent method is the best fit for OsL_2-type complexes.

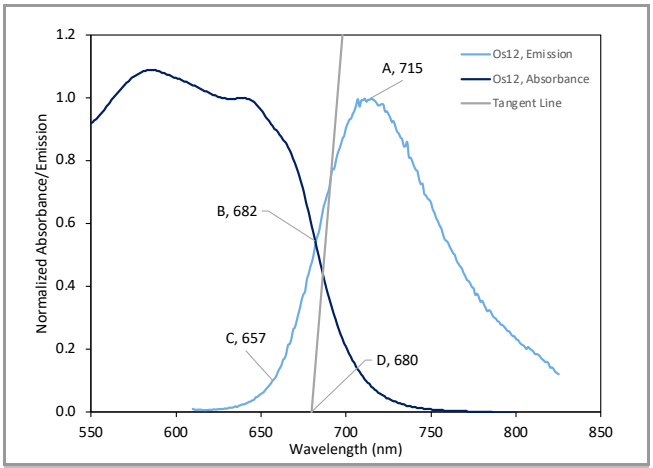

Figure 3 Various methods for approximating the triplet energy of osmium complexes. A) Lambda max of the emission spectrum B) Intersection point of the normalized triplet absorption and triplet emission spectra* C) 10% of the maximum height of the emission spectrum D) x-intercept of the tangent line drawn from the inflection point of the emission spectrum. Measured triplet energy of **Os12** from 77K emission spectrum is 708 nm.[21] *This method was reported in the literature for singlet absorption and emission spectra.

1.4 Synthesis of Osmium Complexes

Two general methods were employed for the synthesis of the osmium complexes reported here (Scheme 1). Complexes **Os1**-**Os19**, **Os23**, **Os24**, and **Os25**- **Os27** were synthesized by Procedure A, using $OsCl_3$ as an osmium source and high temperature (160-230 °C).[4] Serendipitously, the diazafluorenone carbonyl of **Os23** was derivatized by the ethylene glycol solvent to form the acetal. Procedure B using $(NH_4)_2OsCl_6$ and milder reaction conditions (130 °C) proved to be more effective for synthesis of complexes **Os20**, **Os21**, **Os28**, and **Os29**. All complexes were precipitated as the PF_6 salt (except for **Os29** which was isolated as the chloride salt). Recrystallization from acetone with diethyl ether provided pure complexes in most cases. In the case of residual contamination by free ligand, column chromatography could be conducted on neutral alumina to afford the pure complexes.

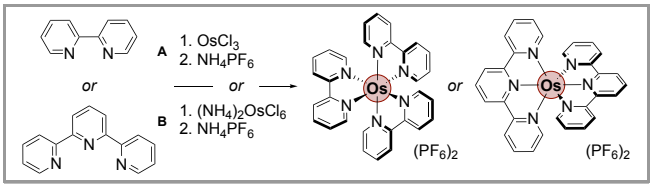

Scheme 1 Procedure A and Procedure B for the synthesis of osmium bipyridyl or terpyridyl complexes.

2 Properties of Osmium Complexes

Herein, we report standardized electrochemical and photophysical properties of 29 osmium complexes, including six which have not been previously reported. Electrochemical and photophysical data for OsL_2 and OsL_3-type complexes are summarized in Tables 1 and 2, respectively. Their structures are shown in Figures 4 and 5. We observed reversible oxidations and quasi- or irreversible reductions for all complexes.

2.1 Redox Potentials of OsL_2-type Complexes

This library contains 15 complexes which are derivatives of $[Os(tpy)_2^{2+}](PF_6)_2$ (**Os4**). When the terpyridine ligand was substituted in the 4'-position with electron donating substituents (both alkyl groups and electron rich arenes), the metal-centered oxidation from Os^{II} to Os^{III} became more facile. This is evident in the negative shift in ground-state potentials of the $Os^{II/III}$ couple. Complexes **Os9** (thiophene, 0.49 V, Table 1, Entry 6), **Os14** (tert-butyl, 0.46 V, Entry 2), **Os15** (4-methoxyphenyl, 0.47 V, Entry 7), and **Os17** (2,4,6-trimethoxyphenyl, 0.44 V, Entry 8) are all negatively shifted relative to **Os4** (0.57 V, Entry 1). Complex **Os8** (furan, 0.52 V, Entry 5) is also negatively shifted, but to a lesser degree. Substituents at the 4'-position which increased the conjugation of the terpyridine ligand, **Os6** (biphenyl, 0.51 V, Entry 3) and **Os7** (naphthyl, 0.52 V, Entry 4), were negatively shifted to about the same degree as **Os8.** Complex **Os10**, which has both a phenyl group in the 4'-position and methyl groups in the 6- and 6''-positions, was also negatively shifted (0.50 V, Entry 9) relative to **Os4**.

Several complexes of osmium and tridentate ligands consisting of electron rich heterocycles were synthesized. The ground state oxidation potential of complex **Os22** (bis-pyrazole, 0.38 V, Entry 16) was significantly negatively shifted from **Os4**, and complex **Os11** (bis-benzimidazole, 0.11 V, Entry 17) had the most negatively shifted $Os^{II/III}$ oxidation potential.

When the terpyridine ligand was substituted in the 4'-position with sigma withdrawing or electron deficient aryl substituents, its oxidation became more difficult. This led to a positive shift in ground state redox potentials. Both functionalizing the terpyridine with an electron withdrawing halogen distally, as in complex **Os3** (4-bromophenyl, 0.59 V, Entry 11), and directly on the 4'-position, as in complex **Os19** (chloride, 0.59 V, Entry 10), positively shifted the oxidation potential to the same extent. Complex **Os18** (pyridine, 0.61 V, Entry 12) showed that electron poor heterocycles in the 4'-position have a similar effect.

Surprisingly, among all the more electron rich derivatives, only **Os22** shows a decrease of ground state reduction potential (-2.10 V, Entry 16) compared to **Os4** (-1.73 V, Entry 1). The reduction potential of complex **Os19** (-1.55 V, Entry 10) as well as **Os3** (-1.62 V, Entry 11) are significantly positively shifted from **Os4**. The reduction potential of **Os3** is in the same range as complexes whose ligands are substituted with electron neutral arenes, **Os6** (-1.62 V, Entry 3) and **Os7** (-1.63 V, Entry 4), which confirmed the observed phenomenon that distal substitution has only marginal effect on redox potential. Following the same trend, complex **Os18** shows a ground state reduction at -1.53 V (Entry 12).

Various tridentate ligands with electron poor pyrimidine scaffolds were synthesized. Three bis-pyrimidinyl analogs of **Os4** were developed with functionalization by an electron rich

Table 1 Electrochemical and Photophysical Properties of OsL_2-type Complexes [a]

Entry	Complex	$E_{1/2}(Os^{III/II})$ (V)	$E_p(Os^{II/I})$ (V)	T_1 (eV)[b]	$E^*_{1/2}(Os^{III/II*})$ (V)	$E^*_p(Os^{II*/I})$ (V)	Echem HOMO-LUMO Gap (V)	λ_{em} (eV)	λ_{abs}/nm (ε*10^{-3}/M^{-1} cm^{-1})
1	**Os4**	0.57	-1.73	1.81	-1.24	0.08	2.3	1.74	279 (44.0), 311 (52.3), 476 (10.6), 539 (4.5), 601 (2.6), 628 (2.8), 660 (3.0)
2	**Os14**	0.46	-1.72	1.80	-1.34	0.08	2.18	1.73	311 (67.6), 481 (17.1), 600 (4.5), 626 (4.6), 656 (4.6)
3	**Os6**	0.51	-1.62	1.76	-1.25	0.14	2.13	1.68	316 (87.8), 492 (36.7), 614 (6.6), 642 (7.7), 669 (9.1)
4	**Os7**	0.52	-1.63	1.78	-1.26	0.15	2.15	1.70	316 (32.8), 493 (14.5), 609 (2.7), 640 (3.2), 665 (3.7)
5	**Os8**	0.52	-1.61	1.72	-1.20	0.11	2.13	1.64	314 (25.2), 498 (11.5), 617 (2.3), 647 (2.7), 675 (3.1)
6	**Os9**	0.49	-1.64	1.75	-1.26	0.11	2.13	1.65	314 (70.5), 492 (27.8), 614 (5.4), 643 (6.3), 669 (7.2)
7	**Os15**	0.47	-1.66	1.76	-1.29	0.10	2.13	1.68	314 (74.2), 493 (28.3), 608 (5.3), 641 (6.3), 669 (7.3)
8	**Os17**	0.44	-1.70	1.77	-1.33	0.07	2.14	1.68	313 (32.5), 492 (13.6), 609 (2.7), 641 (3.2), 670 (3.7)
9	**Os10**	0.50	-1.62	1.73	-1.23	0.11	2.12	1.65	303 (18.3), 392 (1.5), 499 (2.1), 653 (0.7), 683 (0.8), 725 (0.6)
10	**Os19**	0.59	-1.55	1.79	-1.20	0.24	2.14	1.71	325 (21.9), 482 (11.2), 606 (2.9), 638 (3.0), 661 (3.1)
11	**Os3**	0.59	-1.62	1.77	-1.18	0.15	2.21	1.69	283 (71.5), 313 (52.0), 489 (18.1), 610 (3.3), 639 (3.9), 670 (4.6)
12	**Os18**	0.61	-1.53	1.76	-1.15	0.23	2.14	1.67	492 (17.2), 567 (5.9), 610 (4.1), 646 (4.1), 671 (4.5)
13	**Os2**	0.77	-1.45	1.79	-1.02	0.34	2.22	1.70	301 (48.7), 348 (16.6), 484 (25.9), 602 (5.6), 631 (6.0), 658 (6.5)
14	**Os1**	0.65	-1.44	1.78	1.13	0.34	2.09	1.69	306 (42.3), 332 (28.9), 490 (19.3), 603 (5.1), 634 (5.1), 660 (5.3)
15	**Os16**	0.78	-1.40	1.80	-1.02	0.40	2.18	1.71	309 (25.6), 349 (11.4), 482 (15.0), 602 (3.6), 632 (3.6), 658 (3.8)
16	**Os22**	0.38	-2.10	2.14	-1.76	0.04	2.48	2.02	302 (33.2), 387 (15.6), 431 (6.6), 519 (3.2)
17	**Os11**	0.11	-1.70	-	-	-	1.81	-[c]	290 (37.4), 302 (35.9), 314 (36.3), 346 (47.0), 359 (58.2), 487 (16.3), 562 (6.0), 619 (2.4), 778 (1.6)
18	**Os13**	0.78	-1.40	-	-	-	2.18	-[c]	304 (41.6), 339 (64.6), 394 (15.9), 450 (9.2), 498 (6.3)

[a] Counterions are PF_6^- unless otherwise noted. All measurements were taken in MeCN. For electrochemical measurements, all redox potentials are vs. Fc/Fc^+, electrolyte in all cases is 100 mM $TBAPF_6$, the scan rate is 100 mV/s, and all samples were sparged with N_2. [b] T_1 is calculated based on the x-intercept of the tangent line drawn from the inflection point of the emission spectrum. [c] No emission detected upon excitation above 400 nm.

(**Os1**, 4-methoxylphenyl, 0.65 V, Entry 14), neutral (**Os2**, phenyl, 0.77 V, Entry 13), and poor (**Os16**, 3,5-bis(trifluoromethyl)phenyl, 0.78 V, Entry 15) arene and at the 4-position of the central pyridine ring. While all bis-pyrimidinyl derivatives show a significant increase in ground state oxidation potential compared to **Os4**, which can be attributed to the lower energy of the HOMO, the distal functionalization of the arene at the 4-position does not have a significant impact. When turning to the ease of the ground state reduction, complex **Os1** (-1.44 V, Entry 14) and complex **Os2** (-1.45 V, Entry 13) are about the same, whereas complex **Os16** (-1.40 V, Entry 15) is the easiest to reduce. Additionally, a bis-indazole complex, **Os13** (0.78 V, -1.40 V, Entry 18), was synthesized and showed the same ground state redox potentials as **Os16**.

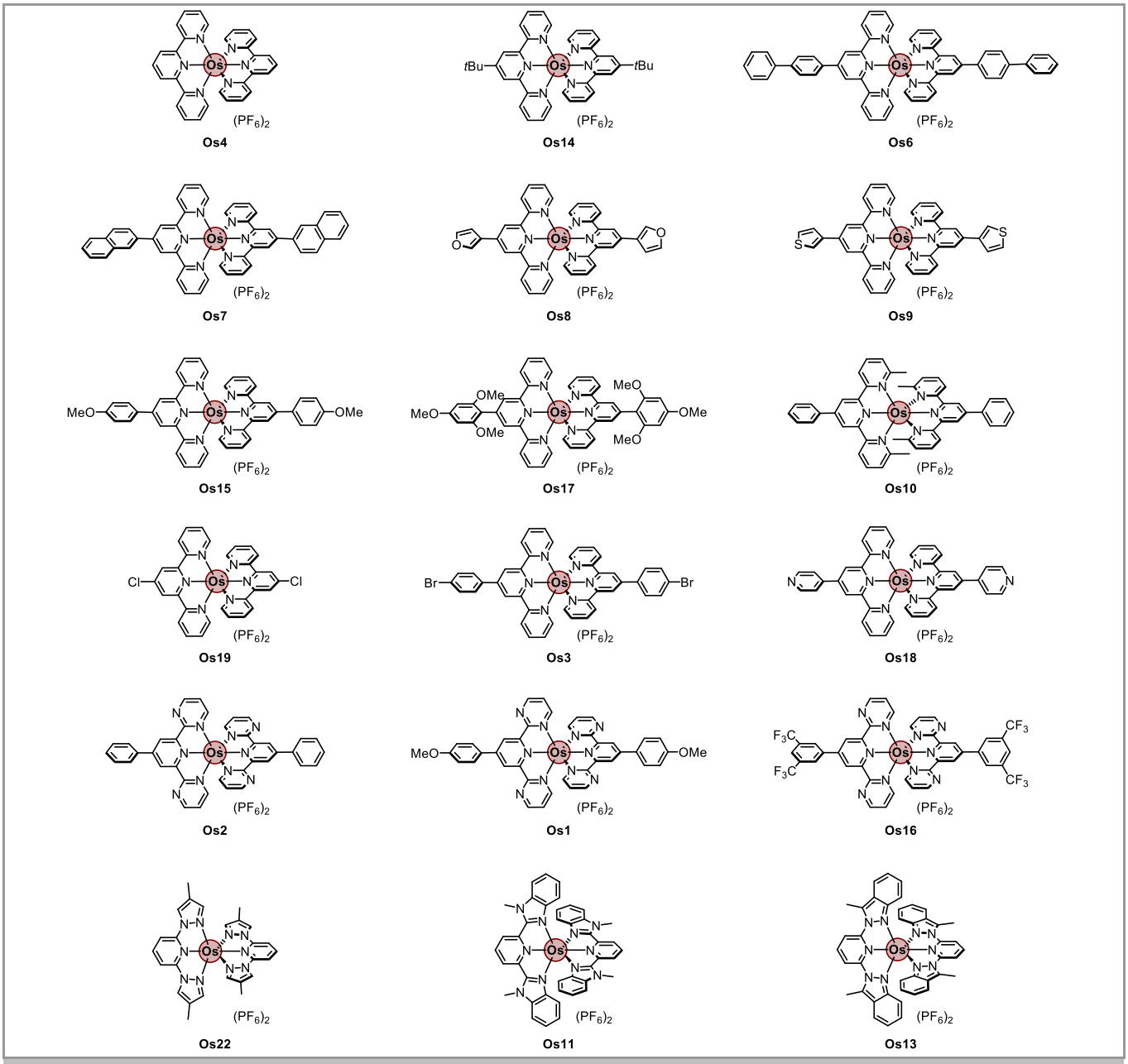

Figure 4 Structures of OsL_2-type Complexes

2.2 Redox Potentials of OsL_3-type Complexes

The remaining 11 complexes in this library are derivatives of $[Os(bpy)_3^{2+}](PF_6)_2$ (**Os12**, Table 2, Entry 1) and $[Os(phen)_3^{2+}](PF_6)_2$ (**Os5**, Entry 9), whose ground state oxidations are the same at 0.44 V. A significant decrease of the oxidation potentials by functionalization of the bipyridine scaffold with electron rich groups was shown on complexes **Os25**, **Os26**, **Os27**, and **Os28**, modified with methyl groups in the 5- and 5'-positions (0.38 V, Entry 2), methyl groups in the 4- and 4'-positions (0.35 V, Entry 3), tert-butyl groups in the 4- and 4'- positions (0.32 V, Entry 4), and methoxy groups in the 4- and 4'- positions (0.07 V, Entry 5) respectively. For the ground state reduction, adding electron donating groups in the 5- and 5'-positions, as in complex **Os25** (-1.87 V, Entry 2), leads to a slightly greater negative shift than adding electron donating groups in the 4- and 4'- positions, as in complexes **Os26** (-1.84 V, Entry 3), **Os27** (-1.84 V, Entry 4), and **Os28** (-1.83 V, Entry 5) relative to **Os12** (-1.68 V, Entry 1).

Modifying the phenanthroline ligand in a similar manner led to an even larger negative shift in potential of the metal-centered oxidation in the case of complex **Os20** (4,4',5,5'-tetramethyl, 0.19 V, Entry 10) and complex **Os21** (5,5'-dimethoxy, 0.01 V, Entry 11). The methyl groups of complex **Os20** (-2.02 V, Entry 10) and methoxy groups of complex **Os21** (-2.06 V, Entry 11) both caused a significant negative shift in the potential of the ground state reductions relative to **Os5** (-1.72 V, Entry 9). A bibenzimidazole complex, **Os29** (-0.07 V, -1.82 V, Entry 6), was also synthesized as a more electron rich analog to bipyridine, and its ground state redox potentials were significantly negatively shifted from **Os12**.

Finally, for electron poor derivatives, a slight positive shift in the ground state redox potentials of **Os23** (diazafluorenone, 0.55 V, -1.66 V, Entry 7) was observed, while a significant shift was observed for **Os24** (bipyrazine, 1.16 V, -1.05 V, Entry 8).

The difference between the formal potential of the oxidation ($E_{1/2}$) and first reduction (E_{pc}) waves, or the electrochemical HOMO-LUMO gap, remained relatively constant across the whole library with an average value 2.14 V and a standard deviation of 0.14 V.

2.3 UV-visible Absorption and Emission Spectroscopy

Both the terpyridyl and bipyridyl osmium complexes studied show sharp, strong absorbance at lower wavelengths, and broad absorbance at higher wavelengths. All complexes except **Os13** and **Os22** can undergo a spin-forbidden direct triplet excitation in the deep-red to NIR 600-700 nm range. The triplet bands of both **Os13** and **Os22** are significantly blue-shifted. Thus, they cannot be excited to T_1 *via* spin-forbidden excitation with NIR light. Orange or green light, however, may be used to achieve this transition. Extinction coefficients of complexes in the range of deep-red and NIR light (600–700 nm) are generally in the range of 1.6–7.3×10^3 M^{-1} cm^{-1} for OsL_2-type complexes and 1.8–4.3×10^3 M^{-1} cm^{-1} for OsL_2-type complexes. Our data suggests that as the substituents on the ligand scaffold are changed, the absorption and emission spectra stay relatively constant. Thus, the electronics of the photocatalysts can be freely tuned without negating the ability of the chromophores to undergo spin-forbidden excitation with NIR irradiation. However, complexes **Os11, Os12,** and **Os29**, bearing benzimidazole (**Os11** and **Os29**) or indazole (**Os13**) heterocycles did not show any emission upon irradiation above 400 nm. Thus, neither their triplet energies, nor their excited state redox potentials could be determined. The non-emissive property of **Os11** was previously described.[22] Literature DFT calculations for complex **Os12** attribute the absorbance feature at 586 nm to the S_0 to T_1 transition.[23] The same authors, as well as others, also assigned the major contribution on the HOMO energy to the osmium metal-center, while ligands are the only contributors on the energy of the LUMO in homoleptic complexes.[7] S_0 to T_1 transition can be thus characterized as metal-to-ligand charge transfer.

Table 2 Electrochemical and Photophysical Properties of OsL_3-type Complexes [a]

Entry	Complex	$E_{1/2}(Os^{III/II})$ (V)	$E_p(Os^{II/I})$ (V)	T_1 (eV)[b]	$E^*_{1/2}(Os^{III/II*})$ (V)	$E^*_p(Os^{II*/I})$ (V)	Echem HOMO-LUMO Gap (V)	λ_{em} (eV)	λ_{abs}/nm (ε*10^{-3}/M^{-1} cm^{-1})
1	**Os12**	0.44	-1.68	1.73	-1.29	0.05	2.12	1.73	299 (33.6), 325 (10.6), 367 (10.3), 388 (9.5), 437 (12.2), 447 (12.2), 479 (12.2), 479 (12.8), 585 (3.5), 639 (3.3), 667 (2.7)
2	**Os25**	0.38	-1.88	1.77	-1.39	-0.11	2.26	1.77	296 (83.9), 374 (9.7), 398 (9.9), 431 (12.4), 471 (13.1), 568 (3.5), 629 (3.2)
3	**Os26**	0.35	-1.84	1.70	-1.35	-0.15	2.19	1.70	291 (67.8), 332 (13.3), 375 (13.7), 393 (12.6), 443 (14.4), 460 (14.8), 488 (15.1), 594 (4.4), 657 (4.0), 680 (3.3)
4	**Os27**	0.32	-1.85	1.71	-1.39	-0.14	2.17	1.71	292 (83.5), 335 (14.0), 376 (14.1), 445 (15.5), 490 (16.1), 589 (4.7), 645 (4.3)
5	**Os28**	0.07	-1.83	1.50	-1.43	-0.33	1.9	1.50	292 (25.6), 341 (12.7), 385 (12.6), 475 (11.1), 509 (10.5), 618 (3.2), 688 (3.0)
6	**Os29**[c]	-0.07	-1.82	-	-	-	1.75	-[d]	278 (66.8), 343 (53.5), 362 (48.4), 532 (11.0), 688 (2.2), 759 (2.1)
7	**Os23**	0.55	-1.66	1.77	-1.22	0.11	2.21	1.77	314 (36.4), 380 (10.0), 427 (12.2), 465 (13.1), 547 (4.6), 625 (4.2), 647 (3.6)
8	**Os24**	1.16	-1.05	1.83	-0.67	0.78	2.21	1.83	302 (14.8), 416 (4.4), 469 (4.6), 553 (2.3), 612 (2.0), 645 (1.8)
9	**Os5**	0.44	-1.72	1.78	-1.34	0.06	2.16	1.78	290 (21.5), 431 (17.0), 475 (15.2), 571 (4.9), 630 (3.8), 651 (3.2)
10	**Os20**	0.19	-2.02	1.81	-1.62	-0.21	2.21	1.81	300 (10.8), 317 (3.9), 333 (4.6), 434 (14.1), 473 (11.8), 559 (4.4), 618 (2.8), 646 (1.9)
11	**Os21**	0.01	-2.06	1.74	-1.73	-0.32	2.07	1.74	296 (31.0), 307 (23.3), 351 (7.5), 372 (8.2), 416 (13.8), 443 (15.9), 463 (15.9), 569 (5.2), 619 (4.2)

[a] Counterions are PF_6^- unless otherwise noted. All measurements were taken in MeCN. For electrochemical measurements, all redox potentials are vs. Fc/Fc^+, electrolyte in all cases is 100 mM $TBAPF_6$, the scan rate is 100 mV/s, and all samples were sparged with N_2. [b] T_1 is calculated based on the lambda max of emission. [c] Counter ions are Cl^-. [d] No emission detected upon excitation above 400 nm.

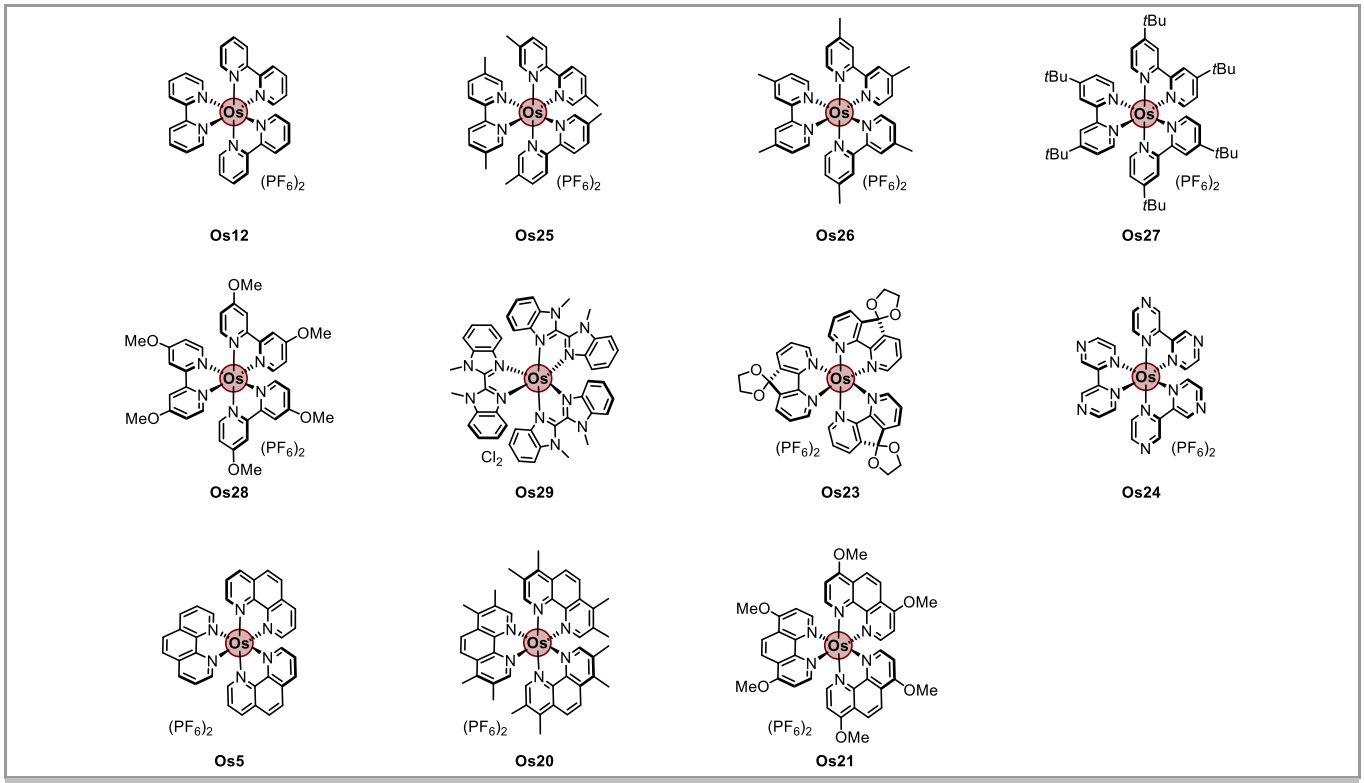

Figure 5 Structures of OsL_3-type Complexes

3 Conclusions

We have reported the synthesis, standardized characterization, and analysis of a library of new and previously reported Os^{II} polypyridyl complexes. We generally observed reversible $Os^{II/III}$ oxidations and quasi-reversible or irreversible reduction waves. The potential of these waves could be modified by tuning the electronics of the ligand scaffolds used. These chromophores have the potential to expand our photocatalytic toolbox to enable broader substrate scope, larger bulk scale, and *in vivo* therapeutic applications. We hope that the consolidation of these properties here will be a useful resource which makes NIR photoredox catalysis more accessible to the synthetic community.

Funding Information

Bristol Myers Squibb

Acknowledgment

EB acknowledges the Experientia Foundation for a postdoctoral fellowship. We are grateful to Bristol Myers Squibb for support.

Supporting Information

YES.

Primary Data

NO.

Conflict of Interest

The authors declare no conflict of interest.

References and Notes

(1) Romero, N. A.; Nicewicz, D. A. *Chem. Rev.* **2016**, *116*, 10075.

(2) Prier, C. K.; Rankic, D. A.; Macmillan, D. W. C. *Chem. Rev.* **2013**, *113*, 5322.

(3) Ravetz, B. D.; Pun, A. B.; Churchill, E. M.; Congreve, D. N.; Rovis, T.; Campos, L. M. *Nature* **2019**, *565*, 343.

(4) Ravetz, B. D.; Tay, N. E. S.; Joe, C. L.; Sezen-Edmonds, M.; Schmidt, M. A.; Tan, Y.; Janey, J. M.; Eastgate, M. D.; Rovis, T. *ACS Cent. Sci*. **2020**, *6*, 2053.

(5) Wang, C.; Zhang, H.; Zhang, T.; Zou, X.; Wang, H.; Rosenberger, J. E.; Vannam, R.; Trout, W. S.; Grimm, J. B.; Lavis, L. D.; Thorpe, C.; Jia, X.; Li, Z.; Fox, J. M. *J. Am. Chem. Soc.* **2021**, *143*, 10793.

(6) Thompson, D. W.; Ito, A.; Meyer, T. J. *Pure Appl. Chem*. **2013**, *85*, 1257.

(7) van der Westhuizen, D.; Conradie, J.; von Eschwege, K. G. *Electroanalysis* **2020**, *32*, 2838.

(8) A, L.; J, A.; J, W. *Bioelectrochemistry* **2005**, *67*, 1.

(9) Liu, Y.; De Nicola, A.; Reiff, O.; Ziessel, R.; Schanze, K. S. *J. Phys. Chem. A* **2003**, *107*, 3476.

(10) Wang, J. *Analytical Electrochemistry*; 2nd ed.; John Wiley & Sons, Ltd: New York, **2000**.

(11) Bard, A. J.; Faulkner, L. R. *Electrochemical Methods: Fundamentals and Applications*; Harris, D.; Swain, E., Eds.; 2nd ed.; John Wiley & Sons, Ltd: Austin, **2004**.

(12) Elgrishi, N.; Rountree, K. J.; McCarthy, B. D.; Rountree, E. S.; Eisenhart, T. T.; Dempsey, J. L. *J. Chem. Educ.* **2017**, *95*, 197.

(13) Gritzner, G.; Kuta, J. *Pure Appl. Chem.* **1984**, *56*, 461.

(14) Jones, W. E.; Fox, M. A. *J. Phys. Chem*. **1994**, *98*, 5095.

(15) Oda, N.; Tsuji, K.; Ichimura, A. *Anal. Sci.* **2001**, *17*, 375.

(16) Riis-Johannessen, T.; Dupont, N.; Canard, G.; Bernardinelli,

G.; Hauser, A.; Piguet, C. *Dalton Trans.* **2008**, *9226*, 3661.
(17) Johnson, S. R.; Westmoreland, T. D.; Caspar, J. V.; Barqawi, K. R.; Meyer, T. J. *Inorg. Chem.* **1988**, *27*, 3195.
(18) Wei Xu; Bo Peng; Jun Chen, *; Mao Liang, and; Cai, F. *J. Phys. Chem. C* **2008**, *112*, 874.
(19) Till, N. A.; Tian, L.; Dong, Z.; Scholes, G. D.; MacMillan, D. W. C. *J. Am. Chem. Soc.* **2020**, *142*, 15830.
(20) Kandoth, N.; Hernández, J. P.; Palomares, E.; Lloret-Fillol, J. Sustain. *Energy Fuels* **2021**, *5*, 638.
(21) Ondongo, O. S.; Endicott, J. F. *Inorg. Chem.* **2009**, *48*, 2818.
(22) Shao, J. Y.; Zhong, Y. W. *Inorg. Chem.* **2013**, *52*, 6464.
(23) Yaxiong Wei; Min Zheng; Lin Chen; Xiaoguo Zhou; Shilin Liu *Dalton Trans.* **2019**, *48*, 11763.